JOURNAL OF AIRCRAFT
Vol. 41, No. 5, September–October 2004

Numerical and Experimental Study of Flow Structure of Low-Aspect-Ratio Wing

Tang Jian* and Zhu Ke-Qin†
Tsinghua University, 100084 Beijing, People's Republic of China

Unsteady aerodynamic characteristics of a low-aspect-ratio elliptic wing with an E-174 aerofoil are studied by numerically solving unsteady incompressible Navier–Stokes equations. Two phenomena have been found: The first phenomenon is found at angle of attack larger than 11 deg, where the flow around the wing becomes bilateral asymmetric. This phenomenon is caused by tip vortices' destabilization. Tip vortices' destabilization is due to interaction between a secondary separated vortex and the tip vortices. The second phenomenon is found at angle of attack larger than 33 deg, where a large separated vortex stays above the wing, forming a stationary vortex. The stationary vortex is thought to be related to the vertical component of the tip vortices. Experimental flow visualization has verified the phenomena found in the numerical simulation.

Nomenclature

AR	=	aspect ratio, based on maximum chord
c	=	chord length at the mid of the elliptical wing
Re	=	Reynolds number, Uc/v
t	=	physical time
$\bar{t}$	=	nondimensional time, tU/c
U	=	final constant speed of wing

Introduction

In recent years, research of micro-air-vehicles (MAVs) has attracted extensive interest. Because of their small size and low speed, MAVs' chord Reynolds numbers ($Re = 10^4$–10^5) are lower than commercial aircraft [$Re = \mathcal{O}(10^7)$]. In the last few decades, the research on low Reynolds number problems had concentrated on two-dimensional airfoils. For instance, McMasters and Henderson[1] found that when Reynolds number increases to about 10^5, the maximum lift-to-drag ratio of airfoils increased dramatically by two orders of magnitude within a narrow Reynolds number range. Mueller[2] also found that lift and drag hysteresis phenomenon occur when the angle of attack or the Reynolds number is recycled. Related research has been documented in Refs. 3 and 4.

Another difference between MAVs' flowfield and a typical commercial aircraft is their three-dimensional characteristics. MAVs have much lower-aspect-ratio wings. Only recently, has research begun on the three-dimensional flowfield of a low-aspect-ratio wing at low Reynolds number. Pelletier and Mueller[5] found in their experiments that flow structures of thin and low-aspect-ratio (AR < 2) wings are different from those of two-dimensional airfoils. As Gad-el-Hak[4] pointed out, the tip vortices play an important role in the flowfield of a low-aspect-ratio wing.

In the present paper, the relations between the tip vortices and flow characteristics of a low-aspect-ratio wing are studied by numerical simulation. The Reynolds number is taken to be 1×10^4. At this Reynolds number, the change of flow structures due to transition and turbulence is avoided, so that the effect of tip vortices is highly weighted in the numerical simulation. The algorithm and the parameters of the numerical simulation are introduced, followed by the results of the numerical simulation. Finally, experimental results are shown to verify the numerical results.

Computational Method

The unsteady incompressible Navier–Stokes equations are solved using an artificial compressibility algorithm developed by Rogers et al.[6] The algorithm introduces a pseudotime derivative of pressure into the continuity equation. Time accuracy in the numerical solutions is achieved by subiteration in pseudotime for each physical time step. The algorithm uses a third-order flux difference splitting technique for the convective terms and a second-order central difference for the viscous terms. The time derivatives in the momentum equation are differenced using a second-order, three-point, backward difference formula. The algorithm is implicit and has second-order spatial and time accuracy.

A code based on the foregoing numerical method has been developed.[7] The accuracy of the code has been verified by analytical solution of the boundary-layer flow on flat plate, by comparison of the calculation and measured pressure distributions on a wing,[7] and further validated by comparison with the three-dimensional unsteady flow experimental results in Refs. 8 and 9.

The mesh was a body-conforming grid generated by solving the Poisson equations. The outer boundary was set at 10 chord lengths from the wing, and the time step was 0.02. A $42 \times 101 \times 49$ grid (in the normal direction, around the wing section, and in the spanwise direction, respectively) was used for the three-dimensional computation. The grid topology used was an O–H type (shown in Fig. 1). The normal grid distance from the wall was 1×10^{-5}. The parameters have been numerical tested and proven good enough to obtain the correct flow structure. A laminar flow model was used in the numerical simulation that relied on the following: an experimental investigation conducted by Traub et al.[10] that showed that no marked transition was observed below $Re = 6 \times 10^4$ and laminar incompressible flow solution results that were obtained by Ghia et al.[11] and Mehta,[12] where their numerical results are in good agreement with the experimental results.

Results and Discussion

Using the described algorithm and grid, a numerical calculation was conducted to study the unsteady flow structure of the wing moving forward with constant speed, $Re = 1 \times 10^4$, and angles of attack from 0 to 45 deg. Numerical calculation was started when the wing accelerated from rest according to the cosine curve $u = 0.5U(1 - \cos \pi \bar{t})$, $0 < \bar{t} < 1$, from 0 to U, and it was stopped when the influence of the startup process disappeared. In the numerical simulation, two phenomena were found: At the angles of attack larger than 11 deg, flow around the wing becomes bilateral

Received 26 September 2003; revision received 2 December 2003; accepted for publication 2 December 2003.

*Postdoctor, Department of Engineering Mechanics; j_tang@sohu.com.
†Professor, Department of Engineering Mechanics.

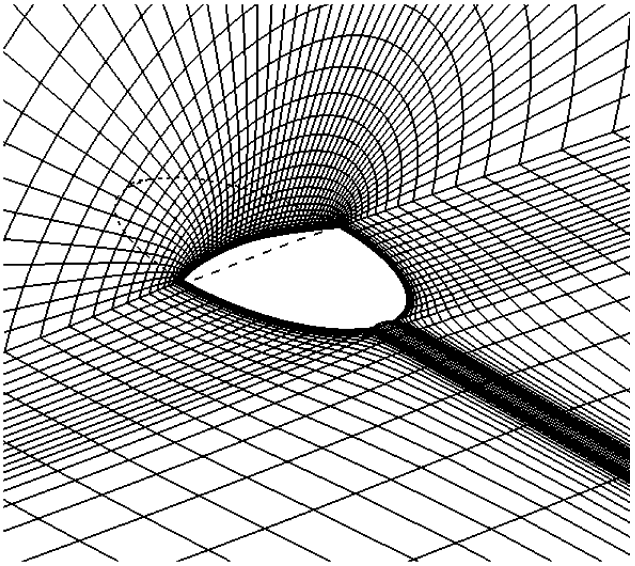

Fig. 1 Grid topology of wing.

asymmetric and at higher incidences (more than about 33 deg), a primary separated vortex is captured over the wing. Flow visualization was conducted and verified the numerical results.

Stationary Vortex Phenomenon

The numerical results show that at angles of attack from 0 to 45 deg separation has taken place at the upper surface. In the separated region, there are three vortices (primary separated vortex, secondary separated vortex, and tail vortex, shown in Fig. 2 as A, B, and C, respectively). When separation takes place at 0-deg angle of attack, the effects of viscosity at low Reynolds number are prominent. As generally known, the primary separated vortices constantly shed. However, behavior of the secondary vortices is different: They shed at around 0-deg angle of attack, whereas at angles of attack larger than 5 deg, they do not shed. As the flow streamlines at midsection of the wing show in Fig. 2, the secondary vortices stay on the upper surface of the wing, at times splitting into two small vortices. The position of the secondary vortex moves upstream on the upper surface of wing with increasing incidence. At 35-deg angle of attack, the secondary vortex is very close to the leading edge of the wing, as shown in Fig. 3.

The primary separated vortices are constantly shed from 0 to 30 deg. (Figure 3a shows the shedding process of the primary vortices at 25-deg angle of attack.) However, at higher incidence, the primary separated vortices stay above the wing instead of shedding into the wake, although their shape and size change with time. Figure 3b shows the flow structures at different time at 35-deg angle of attack. It is clear that the primary vortex is captured above the wing; the secondary vortex stays on the upper surface of the wing, near the leading edge; and tail vortices cyclically produce, grow, and shed into downstream at the trailing edge. From the streamlines in the level plane at the middle of the wing (Fig. 4), it is found that the stationary vortex consists of two counter-rotating vortices. Numerical results indicate that this stationary vortex phenomenon exists at angles of attack from 33 to 45 deg. As generally known the separated vortices above the high-aspect-ratio wings are shed downstream. This stationary vortex phenomenon is a unique phenomenon that accompanies the low-aspect-ratio wing. It is thought that the stationary vortex phenomenon is related to tip vortices based on the following: According to the formula $\boldsymbol{V} = (\boldsymbol{\Omega} \times \boldsymbol{R})/(4\pi R^3)$, the induced velocity produced by the tip vortices is inversely, proportional to the square of the distance R. For the fluid in the separated region above the low-aspect-ratio wing, the distance R is much less than that of typical wings. As a result, the tip vortices' effects on the flow structure of low-aspect-ratio wings are much greater than on common wings.

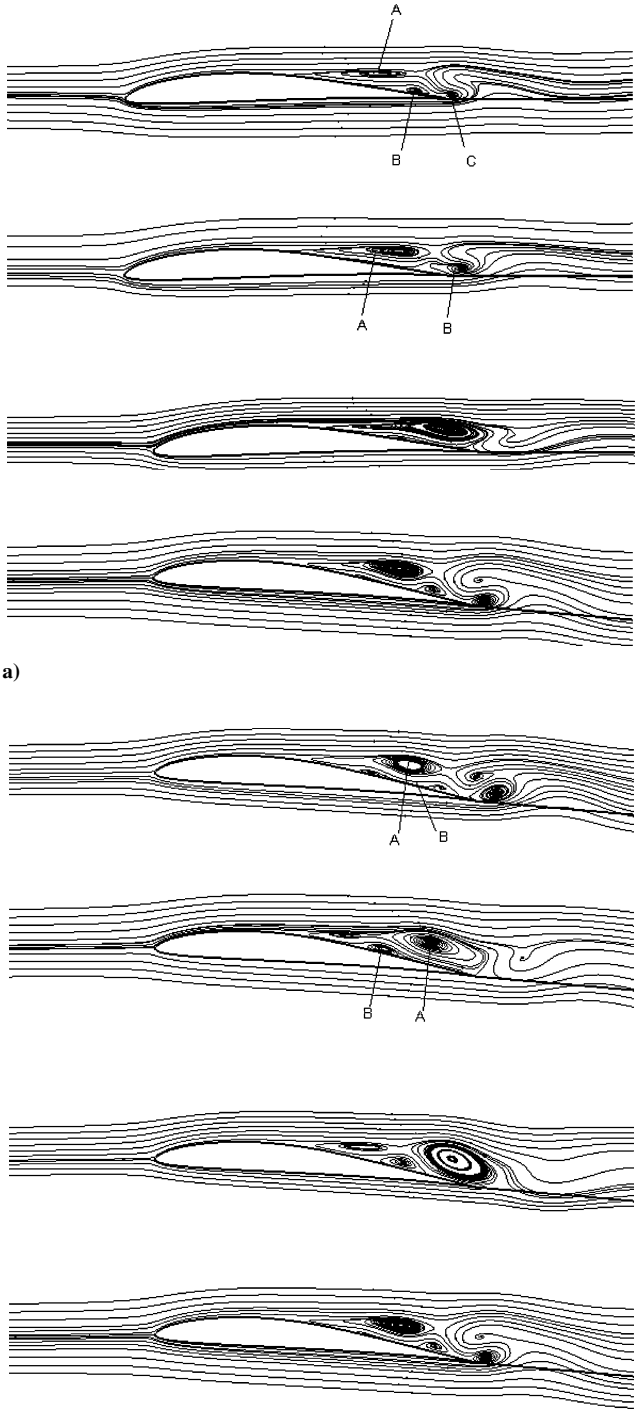

Fig. 2 Flow streamlines at wing midsection at different times: a) 0-deg angle of attack and b) 5-deg angle of attack.

The exact mechanism of this stationary vortex phenomenon requires further study. The vertical components of the tip vortices maybe one of the reasons for this phenomenon: At low incidence, the vertical components of tip vortices cause the separated vortices to move forward, but because the speed of the separated vortex is slower than that of the wing, it is observed to be shedding downstream. As the incidence surpasses the critical angle of attack, the vertical components of tip vortices cause the primary separated vortex to move with the wing, and the separated vortex is observed to stay on the wing.

The stationary vortex above the low-aspect-ratio wing is a new phenomenon. This phenomenon maybe helpful in explaining the existence of the high value of stall angle of attack of low-aspect-ratio wings. Although this stationary vortex is not very strong, the

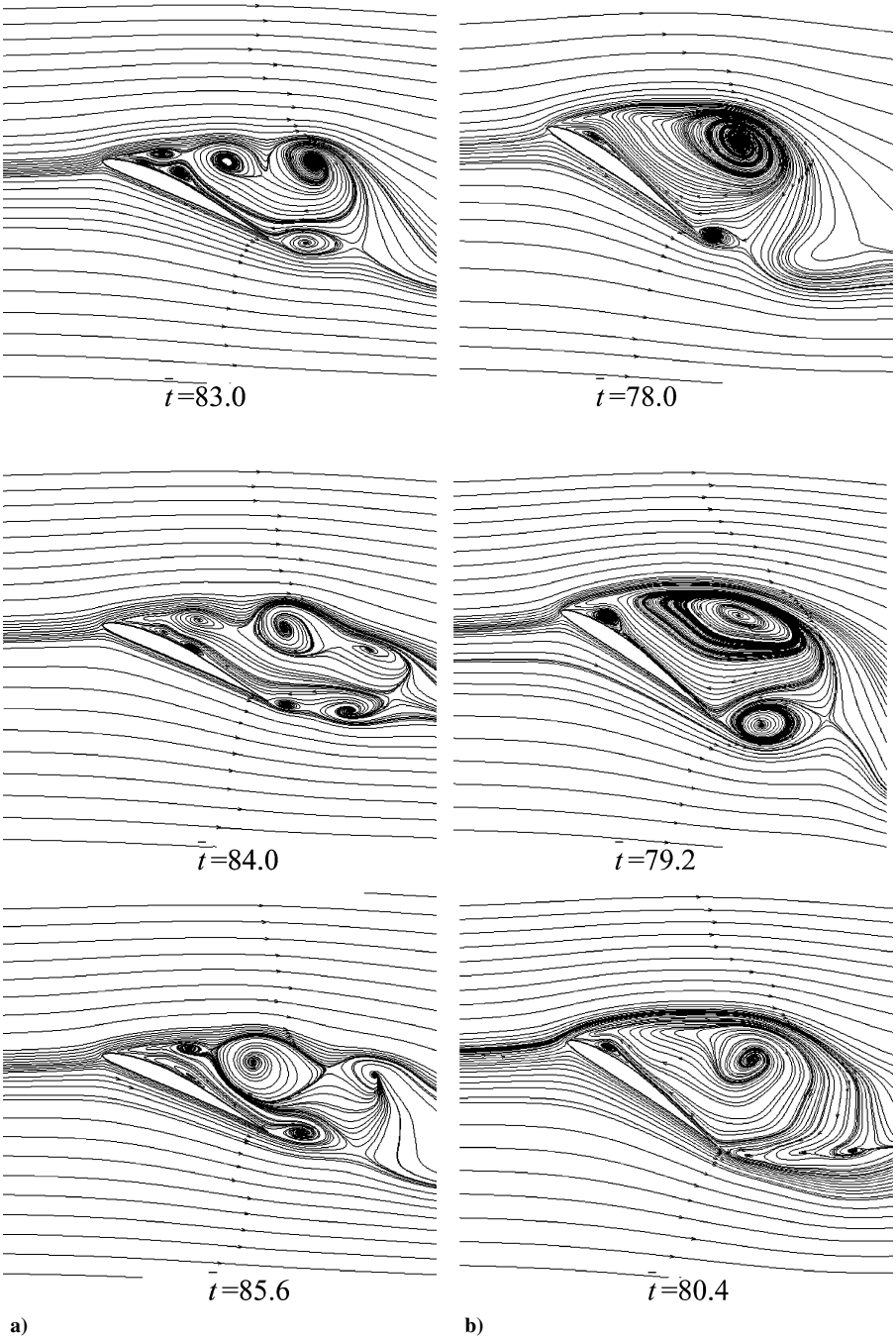

Fig. 3 Flow streamlines at wing midsection at different times: a) 25-deg angle of attack and b) 35-deg angle of attack.

stationary vortex has a potential value in increasing lift and postponing stall.

Bilateral Asymmetry Phenomenon

Figure 4 shows streamlines in the level plane at the middle of the wing at different angles of attack. It can be seen that the flow around the wing is bilateral symmetric at angles of attack up to 10 deg. When incidence is larger than 11 deg, the separated regions above the wing become bilateral asymmetric. Along with the change of the separated region, the tip vortex is bilateral asymmetric and swings from one side to the other side irregularly. Figure 5 shows the position of tip vortices in the vertical plane (trefftz plane) which is $0.5c$ behind the trailing edge at 25-deg angle of attack: At $\bar{t} = 42.0$ (Fig. 5a), the tip vortices swing to left; at $\bar{t} = 54.0$ (Fig. 5b), the tip vortices swing to right; at $\bar{t} = 62.0$ (Fig. 5c), the tip vortices swing back to left again. It is obvious that the tip vortices become instable. Based on numerical results at different angles of attack, the destabilization process of tip vortices may be described as follows (Fig. 6): As the incidence increases, secondary separated vortices stay on the upper surface of the wing at first and then move forward with their spanwise length and strength increasing at the same time. When the incidence surpasses the critical angle, the secondary vortex is close to the tip vortices, and interaction between the secondary vortex and tip vortices exceeds a critical value, after which the tip vortices become instable. This process shows that it is the tip vortices' destabilization that causes the separated region above the wing to become bilateral asymmetric. To prove the numerical calculation obtains a real physical result, a grid was generated, that is slightly bilateral asymmetric. It was then used to repeat the calculations. The results prove that, when the incidence is less than the critical angle, the tip vortices are stable; when the incidence is larger than the critical incidence, the instability of the tip vortices does not change.

This instable phenomenon is important, because it shows a possible stability problem of MAVs. When tip vortices are destabilized,

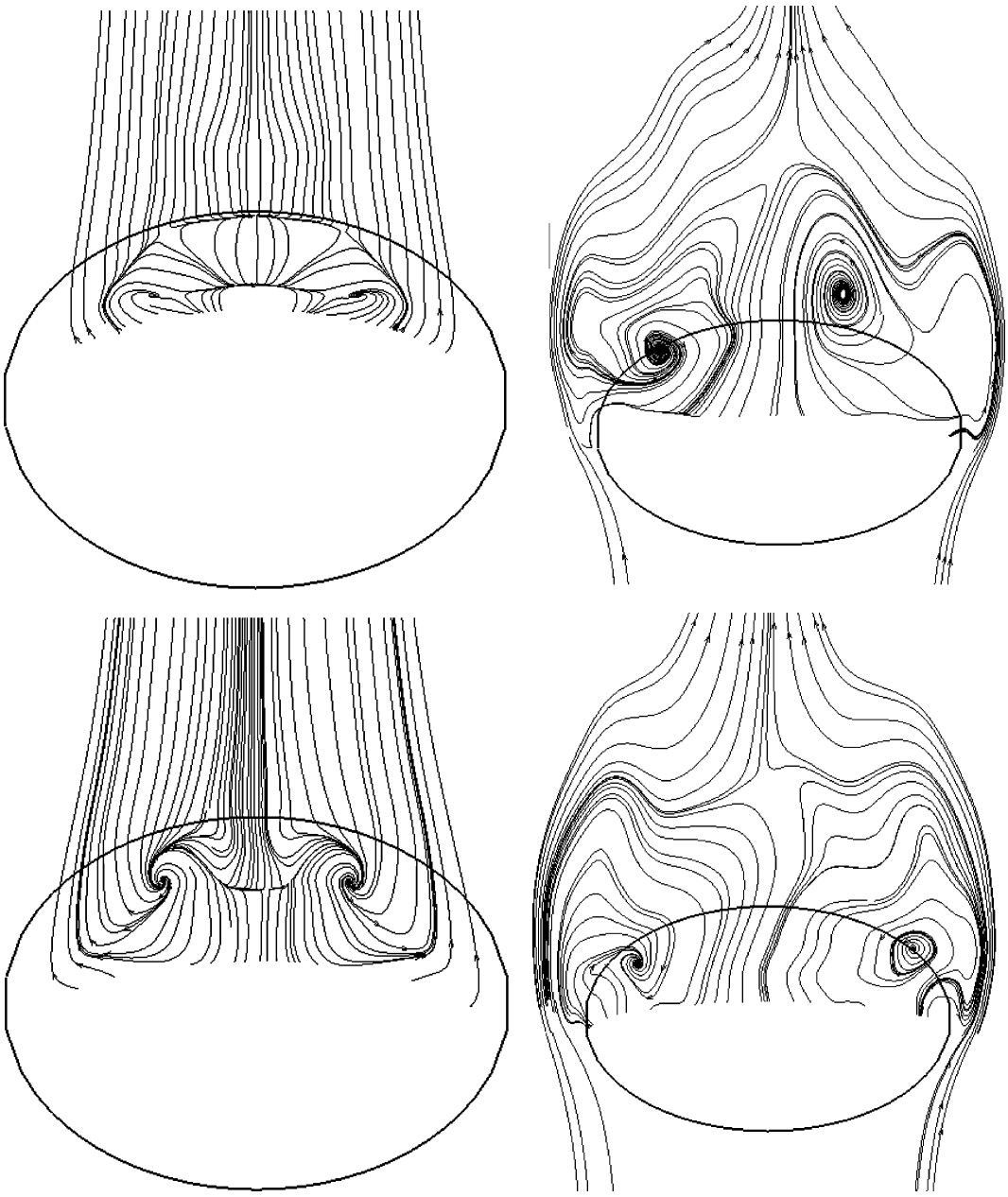

a) b)

Fig. 4 Flow streamlines on the level plane at middle of wing: a) at 5-(top) and 10-deg angles of attack and b) at 35-deg angle of attack of 35 deg, $\bar{t} = 76.0$ (top) and $\bar{t} = 84.0$ (bottom).

the effect is twofold: The asymmetric flow causes unequal drag on each side of the wing, which produces a yawing moment; the asymmetric flow also causes the unequal lift to produce a rolling moment. As a result, the aircraft will suffer spin if its stability is weak or suffer wobbling if its stability is strong, that is, the high swept delta wing. For most MAVs, because of their low-aspect-ratio and low-swept-angle wings, they will be susceptible to spin.

Experiment Results

To verify the foregoing numerical results, flow visualization has been undertaken in the water channel of Beihang University (BUAA). The cross section of the channel is 0.4×0.4 m. In the experiment, the wing and experiment conditions are same as those used in the numerical simulation. Flow was visualized using hydrogen bubbles produced on the upper surface of the wing. Stationary vortex and bilateral asymmetry phenomena were observed in the experiment. To avoid reflection light, photographs were taken slightly in front of the wing; the angle between the span and camera is about 20 deg, which should be considered in comparing the experimental and numerical results. The exposure time was set as 1/10 or 1/20 s; thus, the hydrogen-bubble trajectory could be shown. Because the exposure time is relatively short, the hydrogen-bubble trajectory shows short pathlines in the flow, roughly the flow velocity vector at instant. In this way, the flow visualization photographs can be compared with the flow-streamlines results of the numerical simulation. To describe the vortices more clearly in Figs. 7 and 8, the position and rotation direction of vortices are indicated by arrows based on observation in the experiment. Figure 7 shows the flow structure at 35-deg angle of attack. It can be seen that the positions of primary vortex and secondary vortex coincide with the numerical results. The tail vortices is produced and cyclically shed at the trailing edge. Figure 8 shows the separated region over the wing. It can be seen that at 10-deg angle of attack, flow is bilateral symmetric. At 35-deg angle of attack, flow is bilateral asymmetric, and the size of two vortices change with time.

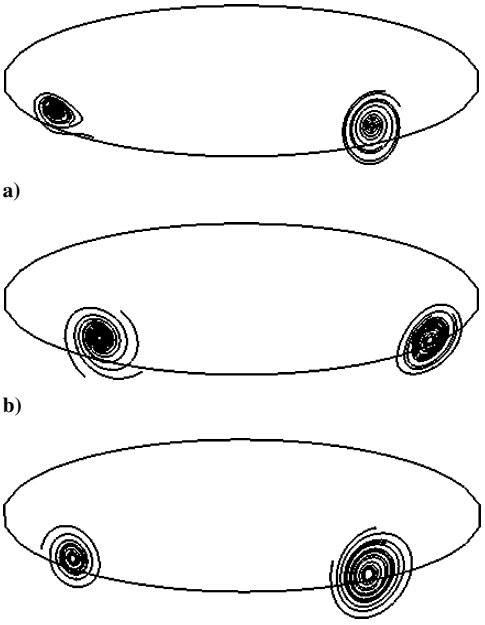

Fig. 5 Tip vortice streamlines in vertical planes (trefftz plane) at about 0.5*c* behind trailing edge at 25-deg angle of attack: a) $\bar{t} = 42.0$, b) $\bar{t} = 54.0$, and c) $\bar{t} = 62.0$.

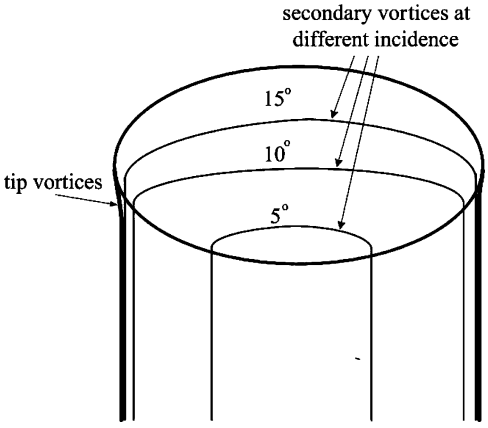

Fig. 6 Schematic of destabilization process of tip vortices; secondary vortices are on upper surface of the wing.

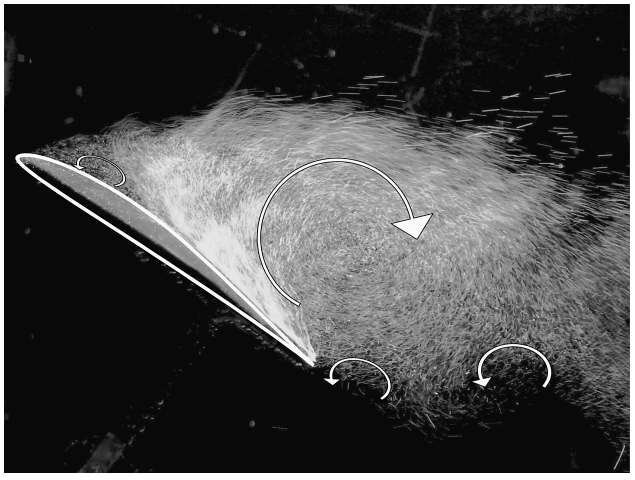

Fig. 7 Flow visualization by hydrogen bubble at 35-deg angle of attack (view from left of the wing).

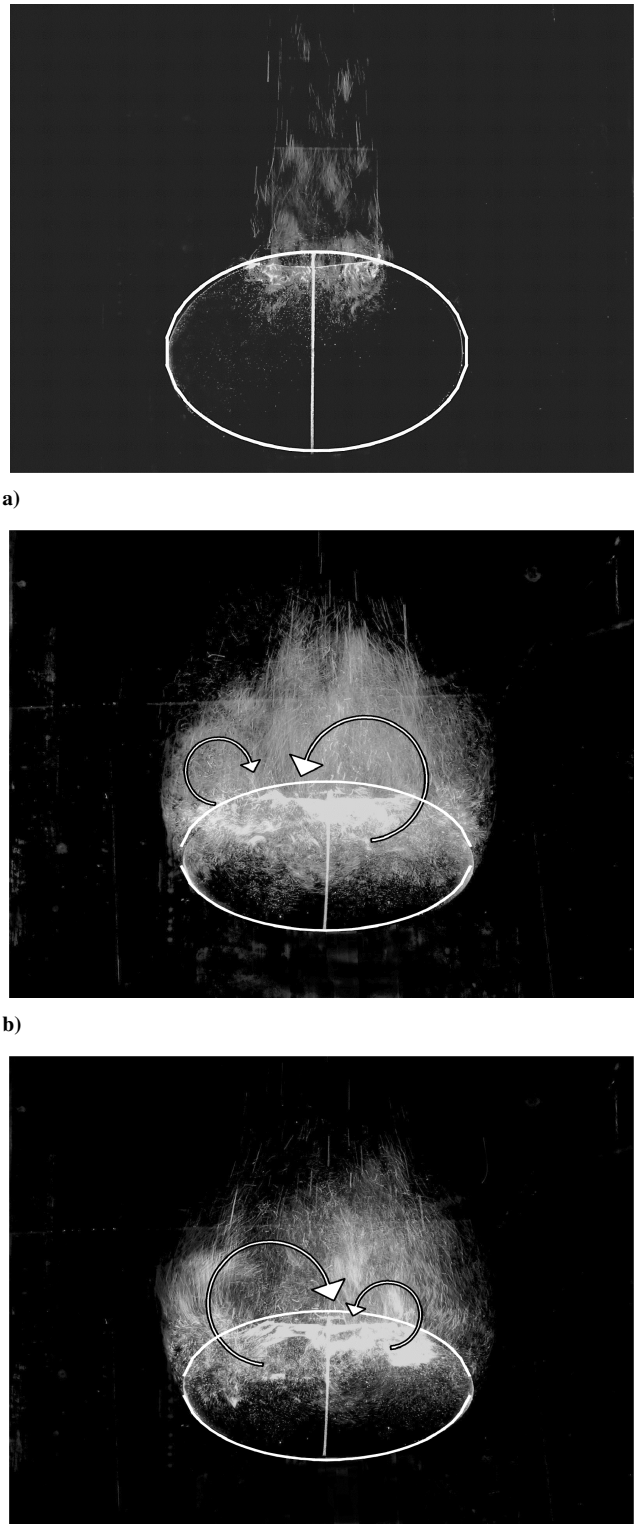

Fig. 8 Flow visualization by hydrogen bubble (view over the wing): a) 10-deg angle of attack and b) 35-deg angle of attack.

Details of the experiment and its results will be discussed in a later paper.

Conclusions

In a numerical study of a low-aspect-ratio elliptic wing with an E-174 aerofoil, the following has been shown: At an angle of attack larger than 11 deg, flow around the wing becomes bilateral asymmetric. This phenomenon is caused by the tip vortices' destabilization. The tip vortices' destabilization is a result of interaction between

the secondary separated vortex and the tip vortices. Separation takes place in the entire range of angles of attack studied in this paper. At angle of attack less than 33 deg, separated vortices above the wing are shed downstream; at high incidence (more than 33 deg), a large separated vortex stays above the wing and forms a stationary vortex. The stationary vortex is thought to be related to the vertical component of tip vortices. Experimental flow visualization has verified the phenomena found in the numerical simulation.

Acknowledgments

The authors gratefully acknowledge Huang Jichi for his helpful comments and consultation. Sheng Gongxin, Tan Guangkun, Zhang Yonggang, and Guo Hui, and others are acknowledged for their helpful support in conducting the experiment in this paper.

References

[1]McMasters, J. H., and Henderson, M. L., "Low Speed Single Element Airfoil Synthesis," *Technical Soaring*, Vol. 6, No. 1, 1980, pp. 1–21.

[2]Mueller, T. J., "Influence of Laminar Seperation and Transition on Low Reynolds Number Airfoil Hysteresis," *Journal of Aircraft*, Vol. 22, No. 9, 1985, pp. 763–770.

[3]Mueller, T. J., and Delaurier, J. D., "Aerodynamics of Small Vehicles," *Annual Review of Fluid Mechanics*, Vol. 35, 2003, pp. 89–111.

[4]Gad-el-Hak, M., "Micro-Air-Vehicles: Can They be Controlled Better?" *Journal of Aircraft*, Vol. 38, No. 3, 2001, pp. 419–429.

[5]Pelletier, A., and Mueller, T. J., "Low Reynolds Number Aerodynamics of Low-Aspect-Ratio, Thin/Flat/Cambered-Plate Wings," *Journal of Aircraft*, Vol. 37, No. 5, 2000, pp. 825–832.

[6]Rogers, S. E., Kwak, D., and Kiris, C., "Numerical Solution of the Incompressible Navier–Stokes Equations for Steady-State and Dependant Problems," *AIAA Journal*, Vol. 29, No. 4, 1991, pp. 603–610.

[7]Lan, S. L., and Sun, M., "Aerodynamic of Properties of a Wing Performing Unsteady Rotational Motions at Small Reynolds Number," *Acta Mechanica*, Vol. 149, 2001, pp. 135–147.

[8]Sun, M., and Tang, J., "Unsteady Aerodynamic Force Generation by a Model Fruit-Fly Wing in Flapping Motion," *Journal of Experimental Biology*, Vol. 205, 2002, pp. 55–70.

[9]Sun, M., and Tang, J., "Energetics of Hovering Flight in *Drosophila Virilus* in Flapping Motion," *Journal of Experimental Biology*, Vol. 205, 2002, pp. 3308–3341.

[10]Traub, L. W., Moeller, B., and Rediniotis, O., "Low-Reynolds-Number Effects on Delta-Wing Aerodynamics," *Journal of Aircraft*, Vol. 35, No. 4, 1998, pp. 653–656.

[11]Ghia, K. N., Yang, J., Oswald, G. A., and Ghia, U., "Study of Dynamic Stall Mechanism Using Simulation of Two-Dimensional Navier–Stokes Equations," AIAA Paper 91-0546, 1991.

[12]Mehta, U. B., "Dynamics Stall of an Oscillating Airfoil," CP-227, No. 23, AGARD 1977.